2025 IEEE World Haptics Conference (WHC)
Suwon Convention Center, Suwon, Korea
July 8 ~ 11, 2025

Capturing 3D Skin Deformation and Finger Kinematics in Active Touch with Compliant Materials

J. Michael Bertsch
Department of Systems and Information Engineering
University of Virginia
Charlottesville, VA USA
xyp5sj@virginia.edu

Anika R. Kao
Department of Mechanical and Aerospace Engineering
University of Virginia
Charlottesville, VA USA
ak4hz@virginia.edu

Gregory J. Gerling
Department of Systems and Information Engineering
University of Virginia
Charlottesville, VA USA
gg7h@virginia.edu

***Abstract*—In touch interactions with compliant materials, such as soft fruits and tissues, an individual's finger movements elicit unique and nuanced cutaneous and kinesthetic cues. The qualities of such cues are key to our perceptual judgments, but due to the spatiotemporal complexity of human touch, its contact interactions are difficult to capture and analyze. Prior efforts to quantify these cues have mostly been limited to passive touch, which constrains one's finger orientation, point of contact, forces, and displacements. Moreover, studies in active touch paradigms often only consider contact with rigid plates. This work describes a novel approach to measure cutaneous skin deformation and kinesthetic digit movements while exploring compliant materials in active touch. We use digital image correlation to track 3D skin surface deformation and quantify its compressive and tensile strain, cross-sectional curvature, and contact area. Additionally, optical sensors are used to track digit movements and quantify their joint angles, normal displacement, penetration depth, and applied force. We measure the effects of varying stimulus compliance (45 and 184 kPa elastomers) on active contact in human-subjects experiments and identify that participant-specific trajectories indeed generate differentiable changes across several skin deformation cues.**

Keywords—active touch, skin mechanics, compliance, softness

I. Introduction

Our unconstrained, volitional exploration of objects in our environment facilitates their perception, where we instinctively move our fingers to differentiate objects through touch. For example, humans apply pressure to ascertain the compliance of soft surfaces and lateral motion to ascertain texture. Such interactions were defined in Klatzky and Lederman's "exploratory procedures" [1]. Subsequent work explains that our tactile judgements rely upon correctly eliciting a combination of perceptual cues arising from both kinesthetic (proprioceptive afferents in joints and muscles) and cutaneous (mechanoreceptive afferents in skin) sources [2],[3],[4],[5]. An improved definition of such cues promises to clarify design requirements for the next generation of immersive haptic displays (e.g., to dynamically vary material compliance [6]).

Most of our understanding of cutaneous cues in compliant interactions comes from measurements of skin deformation in passive touch. In passive touch interactions, a moving stimulus is delivered to the stationary skin, relying completely on the mechanical information received by the skin at the point of contact. Conversely, active touch allows for the direct modulation of contact trajectory and force based on sensory information from the joints and muscles, communicating the relative movement of the body in space. The study of passive touch is also somewhat unnatural, as it necessitates highly controlled and constrained finger orientations, points of contact, forces, and displacements [7], [8], [9]. In contrast, prior active touch efforts have measured skin deformation, but are so far limited to contact with rigid, glass plates [9], [10], [11]. Others have examined active touch with compliant materials in more complex interactions like pinching and squeezing [12], [13], although many of these works measure kinesthetic cues in finger movements, as opposed to skin deformation [14]. As we have learned with compliant materials, it is the confluence of cutaneous cues (i.e., the rate of change of contact area [8], [15], among others) and kinesthetic cues that jointly drive our perceptual acuity [16], [17]. Overall, our understanding of the skin's deformation in response to compliant interactions remains unexplored in active touch.

Our existing knowledge of the cutaneous and kinesthetic cues central to active touch is derived from psychophysical and biomechanical studies with human participants. This includes kinesthetic metrics that may be integral to our active perception of compliance, including penetration depth and the angle of the finger pad and the rotation about the metacarpophalangeal joint [18], [19]. Select studies have begun to examine strategies for modulating these kinesthetic cues, showing that one's applied force may help attain higher differential sensitivity, and that the use of a steeper joint angle is typical when discriminating stiffer surfaces [3], [20]. For cutaneous skin deformation cues, a combination of contact area [21], indentation depth [22], contact force [23], tensile and compressive strain [24], and corresponding temporal dynamics [8], [25] are believed to help encode material compliance. Only recently have highly accurate optical techniques been implemented to measure these cues, though to-date they have been used exclusively in passive touch paradigms [26], [27], [28].

This work describes a novel approach to measure cutaneous and kinesthetic cues when exploring compliant materials in active touch. Using transparent, compliant substrates of varying compliance, we image through stimuli to the skin's surface throughout the duration of contact. Utilizing digital image correlation (DIC), we measure deformation and strain fields of the skin's surface, while additional optical tracking methods allow us to measure the volitional kinesthetic cues (e.g., joint angle and penetration depth). Three studies were performed to demonstrate and validate our ability to measure unconstrained

This work was supported in part by the U.S. National Institutes of Health under Grants R01AT013186, R21AT011980, U24AT011969, and U24AT011970.

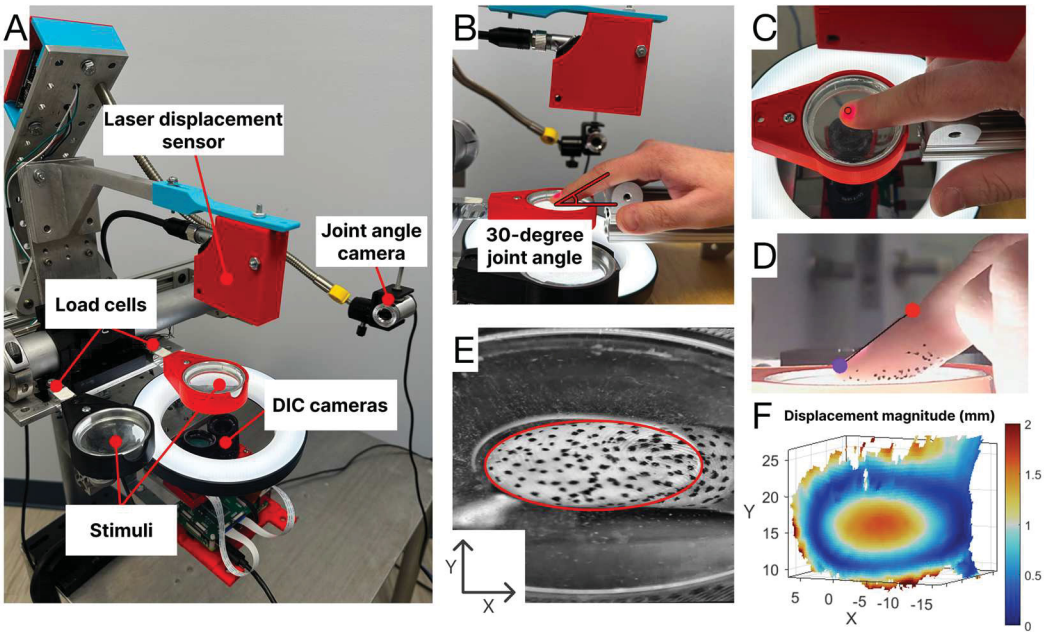

Fig. 1. Experimental setup for active touch interactions with compliant substrates. (A) Participants freely control their applied force to fixed stimuli. Single-axis load cells attached to compliant transparent stimuli (45 and 184 kPa shown) record contact force. A stereo camera pair positioned beneath the stimulus captures synchronized images (50 fps) for digital image correlation (DIC), enabling 3D fingertip surface reconstruction and deformation measurements. (B) Side view of the participant's index finger engaging the stimulus at approximately a 30-degree joint angle, recorded by a side-view camera and quantified using open-source body tracking software. (C) A laser displacement sensor positioned above the setup measures fingertip displacement and provides visual feedback to ensure the participant maintains a position in the center of the stimulus. (D) Joint angle is calculated by fitting a line between the fingertip (purple) and distal interphalangeal joint (red). The angle of this line relative to the horizontal plane is then determined. (E) Paint speckles applied manually to the fingertip create a unique pixel pattern for precise tracking of skin surface deformation by DIC. The red oval highlights the approximate contact area between the fingertip and the stimulus at a specific time point. (F) 3D heatmap generated by DIC showing displacement magnitude of the fingertip surface at 0.3 s of contact with the 45 kPa stimulus. Maximum displacement (red) occurs at the fingertip center, diminishing radially outward to zero (blue) before increasing again near the periphery.

finger trajectories and the corresponding changes in cutaneous skin deformation cues.

II. Methods

A. Equipment and Experimental Setup

The experimental apparatus (Fig. 1A) was designed to measure kinesthetic and cutaneous cues during active touch interactions with compliant stimuli. Transparent stimuli of varying compliance (45 kPa and 184 kPa) were housed within 3D-printed fixtures and mounted to single-axis load cells (5 kg Strain gauge load cell, Adafruit, USA) to record contact force. The load cells were secured to a translating metal platform, allowing rotation between stimuli, and connected to a microcontroller (Arduino Uno, Arduino, Italy) triggered by the recording PC. A laser displacement sensor (1-micron resolution, optoNCDT ILD 1402-100, Micro-Epsilon, USA) was mounted above the stimuli, with its beam directed at the center of the contact surface to record rigid body displacement of the fingertip. A stereo-camera pair (12 MP, Raspberry Pi High Quality, UK), with wide angle lenses (6 mm Vilros, NJ, USA), connected to a microcontroller (Raspberry Pi, UK), was positioned below the stimuli to capture videos for the image analysis pipeline. An additional side-view camera (Papalook PA150, Shenzhen Aoni Electronic Industry Co., China) recorded the interaction angle and provided visual confirmation of the participant's finger position. All components, including the sensors and cameras, were fixed in position relative to the stimuli to ensure consistent measurements across trials.

Prior to data collection, a high-contrast pattern of randomized speckles was applied to the surface of the skin for tracking with DIC. To ensure proper randomization, contrast, and density of the speckles while minimizing application time, speckles were manually applied with a black, oil-based paint pen (0.3 mm tip), and dried within 60 s. Participants positioned their right index finger in the center of the stimulus (Fig. 1C), described in *II. Methods, C*, with their elbow and forearm flat while seated. The height of the apparatus was adjusted to achieve a 30-degree joint angle between the participant's index finger and the surface of the stimulus (Fig. 2B) measured with a 180-degree protractor to ensure a consistent starting position and orientation between participants.

B. Stimulus Design and Mechanical Properties

Two transparent, compliant stimuli were fabricated. Stimulus 1 was designed to approximate the modulus of human skin (45 kPa) [29], while Stimulus 2 was significantly stiffer (184 kPa). Each stimulus was secured within an aluminum collar (5.4 cm outer radius by 1.6 cm thick) with a glass disc base (5.1 cm radius by 0.3 cm thick) to ensure stability during experiments. Both stimuli were cast from two-component silicone rubbers: Stimulus 1 was made from Solaris (Smooth-on Inc., Macungie, PA, USA), and diluted at a 1:1 ratio with silicone oil (ALPA-OIL-50, Silicone oil V50, Modulor, Berlin, Germany) to achieve lower compliance, while Stimulus 2 was composed of Sylgard 184, Dow Corning, Midland, MI, USA) to provide a higher modulus. The fabrication process and modulus validation followed procedures detailed by Li et al. [8].

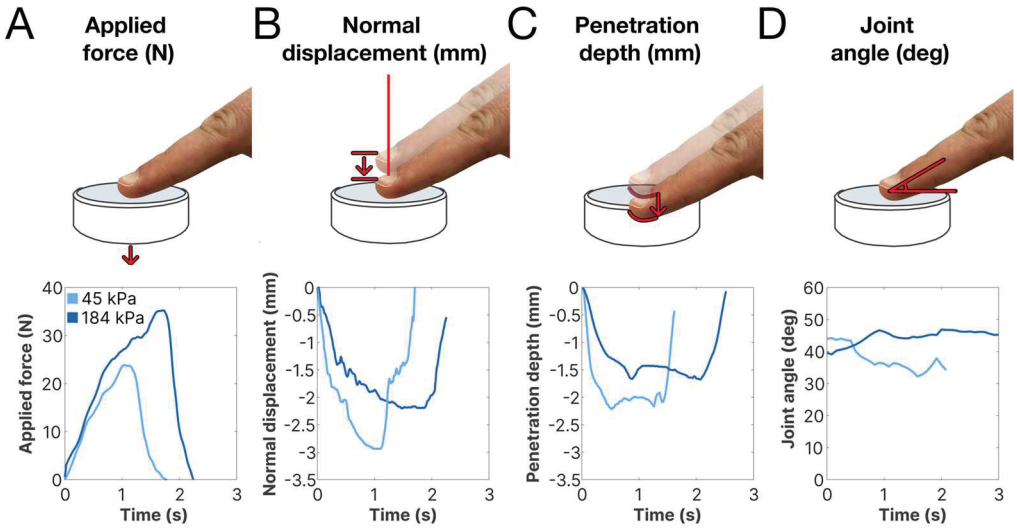

Fig. 2. Kinesthetic cues definitions and examples characterizing active touch interactions with two compliant stimuli. (A) Applied force during active touch is higher and sustained longer for the harder stimulus (184 kPa, dark blue) compared to the softer stimulus (45 kPa, light blue). (B) Normal displacement, defined as rigid body movement of the fingernail in the vertical direction measured by the laser sensor, reaches greater depths for the softer stimulus (-2.92 mm, light blue) than for the harder stimulus (-2.23 mm, dark blue). (C) Penetration depth, the maximum depth of the fingertip skin surface into the stimulus, is also greater for the softer stimulus (-2.20 mm, light blue) compared to the harder stimulus (-1.78 mm, dark blue). The difference between maximum normal displacement and penetration depth remains consistent across stimuli, indicating comparable levels of finger compression. (D) Joint angle deviations are observed during the interaction with both stimuli, with slightly more variability noted for the softer stimulus (range: 32.21 - 44.22 degree) compared to the harder stimulus (range: 39.12 - 52.67 degree).

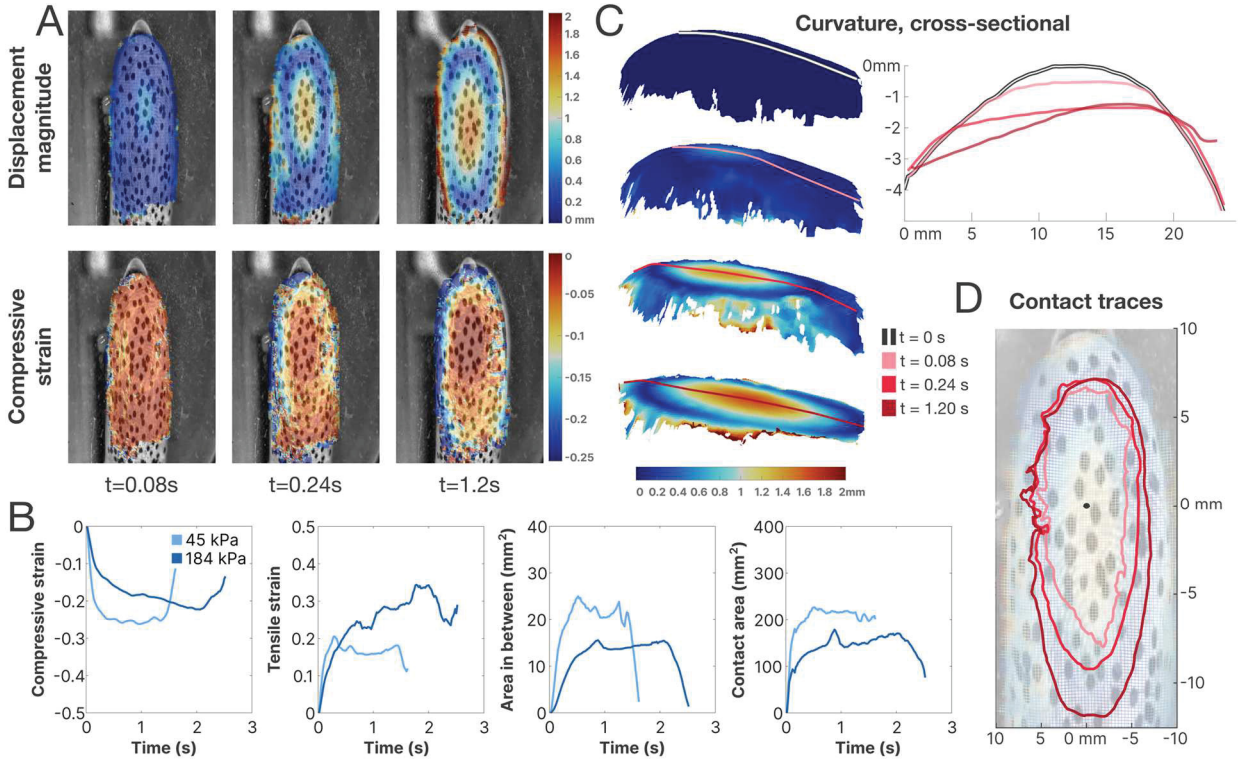

Fig. 3. Cutaneous cue definitions and examples during active touch interactions with two compliant stimuli. Measurements from DIC were used to characterize cutaneous cues, including tensile and compressive strain, area between cross-sectional curvatures, and contact area, during a 2-second trial with 45 kPa and 184 kPa stimuli. (A) Displacement magnitude and compressive strain are overlayed on the finger for three representative time points during indentation with the 45 kPa stimulus: near initial contact (0.08 s), midway through indentation (0.24 s), and sustained maximum indentation (1.2 s). Displacement is highest at the center of the fingertip and tapers to zero radially, marking the area of contact with the stimulus. In contrast, compressive strain is most pronounced near the periphery of the finger, outside the contact zone, with values reaching approximately -0.25. (B) Both stimuli exhibited similar maximum compressive strain values; however, tensile strain magnitudes were greater for the stiffer 184 kPa stimulus. Indentation into the softer 45 kPa stimulus resulted in greater changes in the area between the finger's cross-sectional curvature, reflecting a larger contact area. (C) Fingertip cross-sectional curvature where the black line represents initial curvature prior to contact and red lines show subsequent deformation. Flattening of the fingertip during indentation is quantified by the "area in between" metric, which denotes the area between deformed and initial curves. (D) Contact area was determined by analyzing the 3D displacement point cloud at each time point. Points exceeding the threshold depth of the stimulus defined the extent of contact, and the enclosed area was calculated as the total contact area.

C. Joint Angle Calculation

DeepLabCut [30], [31], a deep learning software tool for marker-less optical point tracking, was used to unobtrusively measure the joint angle of the index finger. This method enabled precise tracking of finger motion without the need for physical markers, reducing experimental interference. A ResNet-50-based neural network was trained using a subset of six manually labeled frames per video (approximately 5% to 20% of frames, depending on video length). The network was trained to track 2D positions of the fingertip and distal interphalangeal joint across the entire trial (Fig. 1D). Side-view videos were recorded at 30 frames per second with a resolution of 1280 by 720 pixels. Each video was input into the trained neural network, which output a .csv file containing frame-by-frame 2D coordinates of the tracked fingertip and joint locations. Using these coordinates, joint angle was calculated in degrees based on pixel location estimates (1).

$$\theta_{joint} = \tan^{-1}\left(\frac{X_{tip}-X_{joint}}{Y_{tip}-Y_{joint}}\right) \quad (1)$$

D. 3D Surface Imaging with Digital Image Correlation

3D digital image correlation (DIC) is a non-contact optical tracking method that utilizes pixel patterns captured by stereo cameras to produce displacement and strain fields [32], [33]. By cross-correlating pixel movement between frames, DIC enables precise tracking of surface deformations. While a single camera can track 2D displacement, a stereo-calibrated pair reconstructs 3D surface deformations by correlating 2D information from both views. Prior to data collection, a stereo camera calibration step is performed to establish the field of view and ensure adequate overlap between the two cameras. Open-source software MultiDIC [32] and Ncorr [33] were used to compute 3D skin surface displacements and strain fields.

For each experiment, synchronized 10-second videos were recorded from the two stereo cameras at 50 fps with a resolution of 1920 by 1080 pixels (~5 pixels/mm). Videos were then trimmed to isolate the contact interactions of interest (~1.5 to 3.5 s), and each frame was converted to greyscale JPEG images for subsequent analysis.

E. Kinesthetic Metric Definitions

Four kinesthetic metrics (Fig. 2) were identified as critical for quantifying active touch: (1) applied force, (2) normal displacement, (3) penetration depth, and (4) joint angle.

Applied force is defined as the force exerted along the axis normal to the stimulus surface, measured in Newtons. *Normal displacement* is defined as the displacement (in millimeters) of the fingertip towards the stimulus, measured by a laser displacement sensor at the back of the fingernail, opposite the contact surface. *Penetration depth* quantifies how far the skin surface deformed into the compliant stimulus. This measurement is derived from DIC point cloud position data relative to a threshold defined by the stimulus surface. Due to measurement noise, penetration depth is represented by the 95th percentile of data points within the point cloud. *Joint angle* describes the contact angle of the fingertip and the distal interphalangeal joint, derived using the optical tracking method described above. While a joint angle of 30 degrees is incorporated into the experimental setup, it is not strictly controlled throughout the experiments.

F. Cutaneous Metric Definitions

Four cutaneous cues were derived to quantify skin surface deformation: (1) compressive strain, (2) tensile strain, (3) area between cross-sectional curvature, and (4) contact area.

Compressive and tensile strain quantify the localized compression (negative strain) and expansion (positive strain) of the skin surface relative to its initial, undeformed state (Fig. 3A). To account for noise, the 95th percentile of the first and second principal Lagragian strains within the DIC strain fields, respectively, are recorded. *Area between cross-sectional curvature* characterizes normal deformation at the center of the fingertip (Fig. 3C). The undeformed central point is identified by inspection, and cross-sectional curvature was extracted from proximal-to-distal points intersecting this plane. The area between the deformed and initial curvature was then calculated at each time point to quantify deformation. *Contact area* describes the surface area of skin in contact with the stimulus. Using 3D displacement data, a predefined threshold was set at the stimulus surface, and points below this threshold are filtered out. A perimeter is then drawn around the remaining points to outline the contact region at each timestep (Fig. 3D) and contact area is calculated from this perimeter.

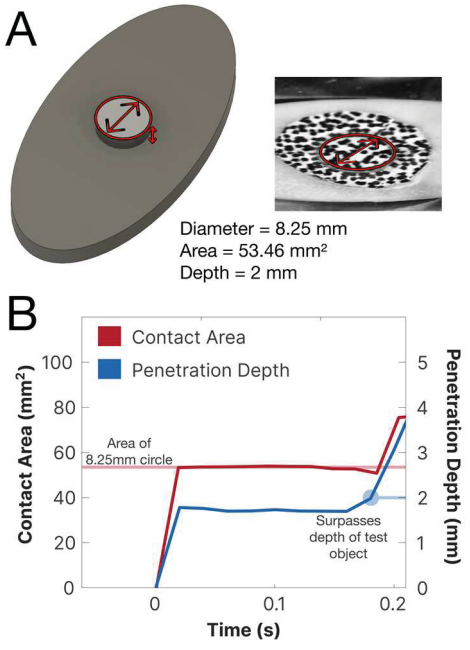

Fig. 4. Validation of DIC contact area measurement using custom-designed test object. (A) Flat, elliptical, 3D-printed test object (25 mm width, 50 mm length) with a cylinder protruding from the center (8 mm diameter, 2 mm depth). A speckle patterned sticker was applied to the top of the cylinder to enable DIC tracking. The addition of the sticker slightly increased the cylinder diameter (8.25 mm), resulting in a surface area of 53.46 mm^2. (B) The test object was indented 2 mm into the 45 kPa stimulus. Measured contact area was 53.4734 mm^2, indicating high accuracy (0.02% error) that remained constant until indented beyond the maximum depth of the test object.

III. Experiments

Three experiments were performed to validate and test the capabilities of this system. Two participants with varying finger size and stiffness were recruited for Experiments 2 and 3. Participant 1 was male with stiffer, calloused skin, whose index finger measured 17.5 mm wide. Participant 2 was female, whose index finger measured 16.0 mm wide. It is important to note that though an initial joint angle of 30 degrees was calibrated for participants prior to each experiment, participants did not, and were not required to, maintain that angle throughout the trial.

A. Experiment 1: Validation of Tracking with a Test Object

In this experiment, we sought to validate the optical tracking and measurement methods using a rigid object of known dimensions. A 3D-printed test object was built, consisting of a flat 25x50 mm plate with an 8 mm-diameter cylinder protruding a height of 2 mm out from the center. The cylinder was covered with a speckled sticker for tracking with DIC, increasing its diameter to 8.25 mm. This resulted in a test object with a known contact area of 53.46 mm^2 and maximum penetration depth of 2 mm before connecting with the base plate (Fig 4A). To validate tracking and contact area calculations through the compliant stimuli, the test object was indented less than 2 mm into Stimulus 1 and held steady before indenting further.

B. Experiment 2: Normal Indentation into Compliant Stimuli

In this experiment, we aimed to measure the changes in finger trajectory volitionally controlled by Participant 1 in direct response to the stiffness of the stimulus. Participant 1 had no contact or training with the different stimuli prior to this experiment and was tasked with indenting his finger pad into the stimulus for approximately 2 s while maintaining the 30-degree joint angle. No instructions were given to suggest a force, displacement, or indentation velocity, and no real-time measurements were displayed to the participant or experimenter. The participant simply received a verbal "begin" command. The experiments were manually trimmed based on the onset and offset of contact with the stimulus from the original 5-second recordings.

C. Experiment 3: Repeated Indentations between Participants

This experiment evaluated the consistency of two participants across four identical, repeated trials. Participants completed this experiment following completion of Experiment 2, meaning they had already made initial contact with the stimulus. The instructions for Experiment 3 were consistent with Experiment 2: to indent the finger pad into the 45 kPa stimulus for approximately 2 s while maintaining the 30-degree joint angle without any external feedback to the subject or experimenter. However, following each indentation participants were instructed to repeat the task and to be as consistent as possible. A mandatory break of 60 s also preceded each subsequent trial.

IV. Results

A. Experiment 1: Validation of Tracking with a Test Object

Indenting the test object less than 2 mm into the 45 kPa stimulus resulted in high accuracy, with an average contact area of 53.47 mm^2, a 0.02% error compared to area of the test object, 54.46 mm^2. As penetration depth surpassed 2 mm, the surface area rapidly spiked because of the speckling on the base plate of the test object (Fig. 4B). Though this is a rigid object and therefore does not validate deformation-based metrics, it serves as validation of the DIC data collection methods, including camera placement, stimulus construction, and speckle size, and the accuracy of the measurement of displacement and contact area measurements.

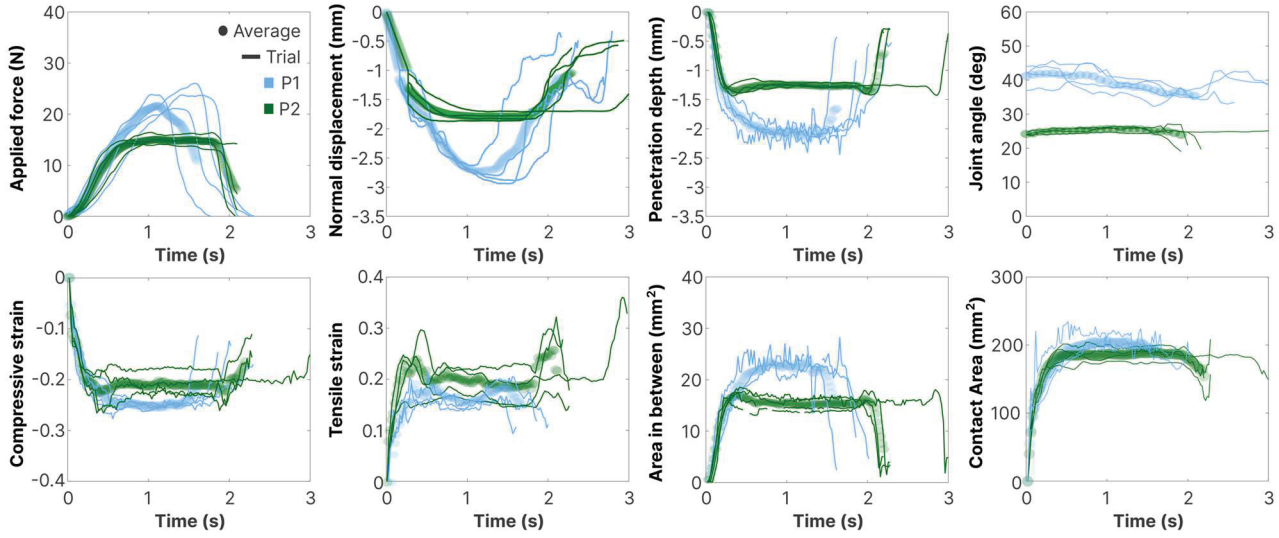

Fig. 5. Individual differences in active touch trajectories between two participants and resultant patterns of skin deformation. Per-trial data (lines) and trial-averaged values (scatter plots) for four repetitions of active touch indentation on the 45 kPa stimulus are shown for two participants (P1: blue, P2: green). Across all active touch metrics, for both kinesthetic cues (top row) and cutaneous cues (bottom row), participants were distinct from one another, while consistent within self between repeated trials. Participant 1 (male), with a larger, stiffer, and more calloused finger, applied consistently higher forces to the stimulus compared to Participant 2 (female). Consequently, P1 exhibited greater penetration depth and more pronounced deformation of finger curvature. Despite applying higher forces, P1's stiffer skin resulted in lower values of tensile strain relative to P2, whose more compliant (less stiff) finger exhibited higher tensile strain under lower applied forces. Additionally, P1's larger joint angle allowed them to achieve a contact area comparable to that of P2's smaller finger. These findings highlight the role of individual anatomical and mechanical properties in modulating active touch interactions.

B. Experiment 2: Normal Indentation into Compliant Stimuli

The stiffer, 184 kPa stimulus elicited higher maximum applied force of 35.29 N with increased average joint angle of 44.93 degrees compared to 37.64 degrees for the 45 kPa stimulus (Fig. 2), aligning with prior reports [20]. This relationship between contact angle and applied force is highlighted over the first second of contact, as the applied force values follow a consistent slope until approximately 0.5 s, corresponding with the time point at which the contact angles diverge. In contrast, as normal displacement and penetration depth increased for the softer 45 kPa stimulus, joint angle decreased from 44 to 32 degrees (Fig. 2D).

Indentation into both stimuli resulted in similar terminal magnitudes of compressive strain, compressing over 20% relative to the finger's initial length (Fig. 3B), though the softer stimulus achieves this compression much faster. Similar behavior is seen when comparing the disparity between peak normal displacement and penetration depth across compliances, informally measuring the normal compression between the finger pad and fingernail. Conversely, indenting into the stiffer stimulus resulted in far higher tensile strain, with a 36.7% expansion of the finger pad beyond its initial length, compared to a 22.7% increase with the soft stimulus. Indentation into the softer stimulus also led to greater change in the area between cross-sectional curvatures of the finger at 25.9 mm^2, which may relate to the increased contact area (234.4 mm^2).

C. Experiment 3: Repeated Indentations between Participants

Participant 1's larger, stiffer finger pad indented deeper (average penetration depth of 2.2 mm), with an average force 6.6 N higher and joint angle 16 degrees steeper than P2 across repeated trials. This consistently resulted in (1) a higher change in compressive strain, (2) lower tensile strains, (3) larger area in between cross sectional curves, and (4) greater contact area. In comparing kinesthetic measurements across trials, participants exhibit consistent trajectories throughout each interaction with the stimulus. For instance, though the equipment is calibrated to achieve a 30-degree angle with the stimulus, P1 consistently uses a steeper angle, closer to 40 degrees, whereas P2's joint angle flattens more on contact. Similarly, though no instructions regarding applied force are given, the terminal applied force of both P1 and P2 is consistent across trials.

V. Discussion

This work describes a novel approach to measure the cutaneous and kinesthetic cues fundamental to quantifying active touch with compliant objects. By performing human-subjects experiments, this work sought to demonstrate two novel capabilities: (1) the ability to quantify naturalistic, active touch interactions with stimuli of varying compliance, providing time-synchronized data describing how the compliance of stimulus influences kinesthetic adaptations and deformation of the finger pad, and (2) the ability to quantify the strategies used for active touch exploration unique to an individual, consistency across repeated trials, and the differences between individuals.

The first capability is demonstrated in Experiment 2, quantifying how varying an object's compliance affects active touch delivery and corresponding skin deformation. Comparisons between the soft and firm stimuli demonstrate similarities in applied force and joint angle for the first 0.5 s; however, after this point the participant appears to modulate their contact trajectory. This may suggest the time in which the change in stimulus compliance was realized, but formal experimentation is required to verify this. It is also important to note that the higher area in between curves and contact area measurements do not mean the finger is more flattened by the softer stimulus. These area measurements are influenced by the modulation of the joint angle, as a steeper angle reduces the size of the contact surface, and the penetration depth which provides greater contact with the rounded edges of the finger. Though prior work has described the relationship between contact area and applied force, further effort must be devoted to decoding the relationships between active adaptations of the finger trajectory and their direct impact on skin surface deformation and contact.

The second capability is demonstrated in Experiment 3, quantifying the unique strategies and consistency of individual participants across repeated interactions with the same stimulus, as well as the differentiability between participants based on their active touch interactions. Though this experiment is limited to two participants, the capabilities we achieve with this measurement system allow for future expansion of this work to explore statistically discriminable haptic user profiles across broad user populations and stimulus types.

Overall, the development and validation of this approach has proven to be highly accurate, finding a 0.02% error measuring contact area of a rigid test object in Experiment 1. It also allows us to expand on the shortcomings of existing methods to quantify active touch interactions at the finger pad. For instance, using DIC to model the skin's surface affords us the ability to track the displacement of precise points continuously throughout contact, making it possible to accurately derive compressive and tensile strain fields as well as point-wise surface contact for measuring cross-sectional curvature and contact area. By comparison, the disparity mapping approach described by [26] and [8] provides a similar 3D reconstruction of the finger pad, but the 3D points generated are discontinuous for each video frame and therefore can only model 3D position instead of skin deformation. This approach has also only been implemented in a passive touch paradigm with controlled, stationary fingers, which fails to account for natural delivery and controlled adaptations of the finger during interactions. By implementing DIC in active touch, measuring the corresponding finger kinematics, and varying the stimulus compliance, we can begin to quantify the interplay between the contact delivery, skin mechanics, and stimulus properties that is crucial to developing truly immersive haptic displays.

References

[1] S. J. Lederman and R. L. Klatzky, "Extracting object properties through haptic exploration," *Acta Psychologica*, vol. 84, no. 1, pp. 29–40, Oct. 1993, doi: 10.1016/0001-6918(93)90070-8.

[2] J. J. Gibson, "Observations on active touch.," *Psychological Review*, vol. 69, no. 6, pp. 477–491, Nov. 1962, doi: 10.1037/h0046962.

[3] A. Lezkan, A. Metzger, and K. Drewing, "Active Haptic Exploration of Softness: Indentation Force Is Systematically Related to Prediction, Sensation and Motivation," *Frontiers in Integrative Neuroscience*, vol. 12, 2018, Accessed: Feb. 02, 2024. [Online]. Available: https://www.frontiersin.org/articles/10.3389/fnint.2018.00059

[4] M. Cavdan, K. Doerschner, and K. Drewing, "The many dimensions underlying perceived softness: How exploratory procedures are

influenced by material and the perceptual task," in *2019 IEEE World Haptics Conference (WHC)*, Jul. 2019, pp. 437–442. doi: 10.1109/WHC.2019.8816088.

[5] S. S. Kim, M. Gomez-Ramirez, P. H. Thakur, and S. S. Hsiao, "Multimodal Interactions between Proprioceptive and Cutaneous Signals in Primary Somatosensory Cortex," *Neuron*, vol. 86, no. 2, pp. 555–566, Apr. 2015, doi: 10.1016/j.neuron.2015.03.020.

[6] M. Mete, H. Jeong, W. D. Wang, and J. Paik, "SORI: A softness-rendering interface to unravel the nature of softness perception," *Proceedings of the National Academy of Sciences*, vol. 121, no. 13, p. e2314901121, Mar. 2024, doi: 10.1073/pnas.2314901121.

[7] G. Corniani, Z. S. Lee, M. J. Carré, R. Lewis, B. P. Delhaye, and H. P. Saal, "Sub-surface deformation of individual fingerprint ridges during tactile interactions," Jul. 02, 2023, *bioRxiv*. doi: 10.1101/2023.07.02.547395.

[8] B. Li, S. C. Hauser, and G. J. Gerling, "Faster Indentation Influences Skin Deformation To Reduce Tactile Discriminability of Compliant Objects," *IEEE Transactions on Haptics*, vol. 16, no. 2, pp. 215–227, Apr. 2023, doi: 10.1109/TOH.2023.3253256.

[9] B. Delhaye, A. Barrea, B. B. Edin, P. Lefèvre, and J.-L. Thonnard, "Surface strain measurements of fingertip skin under shearing," *Journal of The Royal Society Interface*, vol. 13, no. 115, p. 20150874, Feb. 2016, doi: 10.1098/rsif.2015.0874.

[10] B. Dzidek, S. Bochereau, S. A. Johnson, V. Hayward, and M. J. Adams, "Why pens have rubbery grips," *Proceedings of the National Academy of Sciences*, vol. 114, no. 41, pp. 10864–10869, Oct. 2017, doi: 10.1073/pnas.1706233114.

[11] B. Delhaye, P. Lefèvre, and J.-L. Thonnard, "Dynamics of fingertip contact during the onset of tangential slip," *Journal of The Royal Society Interface*, vol. 11, no. 100, p. 20140698, Nov. 2014, doi: 10.1098/rsif.2014.0698.

[12] H. Z. Tan, N. I. Durlach, G. L. Beauregard, and M. A. Srinivasan, "Manual discrimination of compliance using active pinch grasp: The roles of force and work cues," *Perception & Psychophysics*, vol. 57, no. 4, pp. 495–510, Jun. 1995, doi: 10.3758/BF03213075.

[13] B. Gao, Y. Yu, Y. Ejima, J. Wu, and J. Yang, "The Impact of Task Context on Pleasantness and Softness Estimations: A Study Based on Three Touch Strategies," *Behavioral Sciences*, vol. 15, no. 1, Art. no. 1, Jan. 2025, doi: 10.3390/bs15010063.

[14] C. Xu, S. C. Hauser, Y. Wang, and G. J. Gerling, "Roles of Force Cues and Proprioceptive Joint Angles in Active Exploration of Compliant Objects," in *2019 IEEE World Haptics Conference (WHC)*, Jul. 2019, pp. 353–358. doi: 10.1109/WHC.2019.8816159.

[15] B. Li and G. J. Gerling, "An individual's skin stiffness predicts their tactile discrimination of compliance," *The Journal of Physiology*, vol. 601, no. 24, pp. 5777–5794, 2023, doi: 10.1113/JP285271.

[16] C. Xu, Y. Wang, and G. J. Gerling, "An elasticity-curvature illusion decouples cutaneous and proprioceptive cues in active exploration of soft objects," *PLOS Computational Biology*, vol. 17, no. 3, p. e1008848, Mar. 2021, doi: 10.1371/journal.pcbi.1008848.

[17] W. M. Bergmann Tiest and A. M. L. Kappers, "Cues for Haptic Perception of Compliance," *IEEE Transactions on Haptics*, vol. 2, no. 4, pp. 189–199, Oct. 2009, doi: 10.1109/TOH.2009.16.

[18] M. D. Rinderknecht *et al.*, "Reliability, validity, and clinical feasibility of a rapid and objective assessment of post-stroke deficits in hand proprioception," *J Neuroeng Rehabil*, vol. 15, no. 1, p. 47, Jun. 2018, doi: 10.1186/s12984-018-0387-6.

[19] N. Gurari, K. J. Kuchenbecker, and A. M. Okamura, "Perception of Springs With Visual and Proprioceptive Motion Cues: Implications for Prosthetics," *IEEE Transactions on Human-Machine Systems*, vol. 43, no. 1, pp. 102–114, Jan. 2013, doi: 10.1109/TSMCA.2012.2221038.

[20] K. Drewing and M. O. Ernst, "Integration of force and position cues for shape perception through active touch," *Brain Research*, vol. 1078, no. 1, pp. 92–100, Mar. 2006, doi: 10.1016/j.brainres.2005.12.026.

[21] G. Ambrosi, A. Bicchi, D. De Rossi, and E. P. Scilingo, "The role of contact area spread rate in haptic discrimination of softness," in *Proceedings 1999 IEEE International Conference on Robotics and Automation (Cat. No.99CH36288C)*, May 1999, pp. 305–310 vol.1. doi: 10.1109/ROBOT.1999.769996.

[22] C. Dhong *et al.*, "Role of indentation depth and contact area on human perception of softness for haptic interfaces," *Sci Adv*, vol. 5, no. 8, p. eaaw8845, Aug. 2019, doi: 10.1126/sciadv.aaw8845.

[23] M. Liu, A. Batista, S. Bensmaia, and D. J. Weber, "Information about contact force and surface texture is mixed in the firing rates of cutaneous afferent neurons," *J Neurophysiol*, vol. 125, no. 2, pp. 496–508, Feb. 2021, doi: 10.1152/jn.00725.2019.

[24] V. Hayward, A. V. Terekhov, S.-C. Wong, P. Geborek, F. Bengtsson, and H. Jörntell, "Spatio-temporal skin strain distributions evoke low variability spike responses in cuneate neurons," *J R Soc Interface*, vol. 11, no. 93, p. 20131015, Apr. 2014, doi: 10.1098/rsif.2013.1015.

[25] M. A. Srinivasan and R. H. LaMotte, "Tactual discrimination of softness: abilities and mechanisms," in *Somesthesis and the Neurobiology of the Somatosensory Cortex*, P. O. Franzén, P. R. Johansson, and P. L. Terenius, Eds., in Advances in Life Sciences. , Birkhäuser Basel, 1996, pp. 123–135. doi: 10.1007/978-3-0348-9016-8_11.

[26] S. C. Hauser and G. J. Gerling, "Imaging the 3-D deformation of the finger pad when interacting with compliant materials," in *2018 IEEE Haptics Symposium (HAPTICS)*, Mar. 2018, pp. 7–13. doi: 10.1109/HAPTICS.2018.8357145.

[27] A. R. Kao, C. Xu, and G. J. Gerling, "Using Digital Image Correlation to Quantify Skin Deformation With Von Frey Monofilaments," *IEEE Trans. Haptics*, vol. 15, no. 1, pp. 26–31, Jan. 2022, doi: 10.1109/TOH.2021.3138350.

[28] Z. Xu, J. Dela Cruz, C. Fthenakis, and C. Saliou, "A novel method to measure skin mechanical properties with three-dimensional digital image correlation," *Skin Research and Technology*, vol. 25, no. 1, pp. 60–67, 2019, doi: 10.1111/srt.12596.

[29] E. Miguel *et al.*, "Characterization of nonlinear finger pad mechanics for tactile rendering," in *2015 IEEE World Haptics Conference (WHC)*, Jun. 2015, pp. 63–68. doi: 10.1109/WHC.2015.7177692.

[30] A. Mathis *et al.*, "DeepLabCut: markerless pose estimation of user-defined body parts with deep learning," *Nat Neurosci*, vol. 21, no. 9, pp. 1281–1289, Sep. 2018, doi: 10.1038/s41593-018-0209-y.

[31] T. Nath, A. Mathis, A. C. Chen, A. Patel, M. Bethge, and M. W. Mathis, "Using DeepLabCut for 3D markerless pose estimation across species and behaviors," *Nat Protoc*, vol. 14, no. 7, pp. 2152–2176, Jul. 2019, doi: 10.1038/s41596-019-0176-0.

[32] D. Solav, K. M. Moerman, A. M. Jaeger, K. Genovese, and H. M. Herr, "MultiDIC: An Open-Source Toolbox for Multi-View 3D Digital Image Correlation," *IEEE Access*, vol. 6, pp. 30520–30535, 2018, doi: 10.1109/ACCESS.2018.2843725.

[33] J. Blaber, B. Adair, and A. Antoniou, "Ncorr: Open-Source 2D Digital Image Correlation Matlab Software," *Exp Mech*, vol. 55, no. 6, pp. 1105–1122, Jul. 2015, doi: 10.1007/s11340-015-0009-1.